Correcting B0 inhomogeneity-induced distortions in whole-body diffusion MRI of bone metastases

Working Title: Distortion correction in DWI of bone metastases
Word Count: 3246 words

Authors:
Leonardino A. Digma, BA[1*]
Christine H. Feng, MD[1*]
Christopher C. Conlin, PhD[2]
Ana E. Rodríguez-Soto, PhD[2]
Kanha Batra, MS[3]
Aaron Simon, MD, PhD[1]
Roshan Karunamuni, PhD[1]
Joshua Kuperman, PhD[2]
Rebecca Rakow-Penner, MD, PhD[2]
Michael E. Hahn, MD, PhD[2]
Anders M. Dale, PhD[2]
Tyler M. Seibert, MD, PhD[1,2,4]

*Equal contribution

[1]Department of Radiation Medicine and Applied Sciences, UC San Diego School of Medicine, La Jolla, CA, USA
[2]Department of Radiology, UC San Diego School of Medicine, La Jolla, CA, USA
[3]Department of Electrical and Computer Engineering, UC San Diego, La Jolla, CA, USA
[4]Department of Bioengineering, UC San Diego, La Jolla, CA, USA

Correspondence:
Dr. Tyler M. Seibert, MD, PhD
Department of Radiation Medicine and Applied Sciences
Department of Radiology
Department of Bioengineering
University of California San Diego
9500 Gilman Drive, Mail Code 0861
La Jolla, CA 92093-0861
tseibert@health.ucsd.edu

Disclosures:
TM Seibert reports honoraria from Multimodal Imaging Services Corporation, Varian Medical Systems, and WebMD. AM Dale is a Founder of and holds equity in CorTechs Labs, Inc, and serves on its Scientific Advisory Board. He is a member of the Scientific Advisory Board of Human Longevity, Inc. and receives funding through research agreements with General Electric Healthcare. The terms of these arrangements have been reviewed and approved by UCSD in accordance with its conflict of interest policies. ME Hahn reports honoraria from Multimodal Imaging Services Corporation and research funding from General Electric Healthcare.

Acknowledgements:
The authors would like to thank David Karow, MD, PhD and Nathan White, PhD for their contributions toward establishing whole-body diffusion MRI at our institution, as well as Dominic Holland, PhD for his contributions to development of the distortion correction method applied in this work.

Grant Support:
This work was supported by NIH/NIBIB #K08EB026503, American Society for Radiation Oncology, and the Prostate Cancer Foundation. This work was further supported by the National Institute on Aging T35 grant AG26757 (PI: Dilip V. Jeste, MD, and Alison Moore, MD, MPH), and the Stein Institute for Research on Aging and the Center for Healthy Aging at the University of California, San Diego.

Title: Correcting B0 inhomogeneity-induced distortions in whole-body diffusion MRI of bone metastases

Abstract

Background: Accurate imaging of bone metastases is necessary for treatment planning and assessing treatment response. Diffusion-weighted magnetic resonance imaging (DWI) can detect bone metastases, but DWI acquired with echo-planar imaging is susceptible to distortions due to static magnetic field inhomogeneities.

Purpose: Estimate spatial displacements of bone lesions on DWI. Examine whether distortion-corrected DWI more accurately reflects underlying anatomy.

Study Type: Retrospective.

Subjects: 18 patients with prostate cancer bone metastases.

Field Strength/Sequence: 3.0 T; DWI and T2-weighted imaging.

Assessment: We first applied the reverse polarity gradient (RPG) technique to estimate spatial displacements of bone metastasis on DWI. Next, we calculated changes in mutual information (MI) between DWI and T2-weighted images after RPG distortion correction. Further, we annotated skeletal landmarks on DWI and T2-weighted images. RPG was again used to estimate

displacements of these landmarks. Lastly, we calculated changes in distance between DWI- and T2-defined landmarks (i.e., changes in error) after RPG distortion correction.

Statistical Tests: Mean and bootstrap-derived confidence intervals were used to summarize variables that estimate bone lesion distortions. Wilcoxon signed-rank tests were used to assess change in MI between DWI and T2-weighted images after RPG.

Results: Mean (95% CI) displacement of bone lesions was 5.6 mm (95% CI: 4.8-6.5); maximum displacement was 17.1 mm. Corrected diffusion images were more similar to structural MRI, as evidenced by consistent increases in MI after applying RPG (Wilcoxon signed-rank $p<10^{-13}$). Like bone metastases, our annotated skeletal landmarks also underwent substantial displacement (average, 6.3 mm). Lastly, RPG led to consistent error reductions between DWI and T2 for each skeletal landmark (mean, [95% CI]): thoracic vertebrae (-3.8 mm, [-4.3,-3.3]), abdominal vertebrae (-1.0 mm, [-1.2,-0.71]), pelvic vertebrae (-0.6 mm, [-1.0,-0.17]), and femoral head (-1.2 mm, [-2.1,-0.4]).

Data Conclusions: These findings support the use of distortion correction techniques to improve localization of bone metastases on DWI.

Key words: Diffusion-weighted imaging, bone metastasis, reverse polarity gradient, distortion correction, whole-body imaging.

Introduction

Bone is among the most common sites for cancer metastases, especially from primary tumors of the prostate, breast, and lung (1). It is estimated that 5% of cancer patients exhibit metastatic bone disease and that medical expenditure for patients with such disease can reach $12.6 billion for a single year in the United States (2). These metastases are further associated with substantial morbidity from chronic pain, pathologic fracture, and spinal cord or nerve root compression (3).

Accurate characterization of bone metastases is critical for precise staging and treatment planning. Technetium-99m skeletal scintigraphy (often referred to as bone scan), computed tomography (CT), and positron emission tomography (PET) have all been commonly used for detection (4, 5). More recently, diffusion-weighted magnetic resonance imaging (DWI) has garnered attention for its potential in evaluating bone metastases (6, 7). DWI has the advantages of increased spatial resolution compared to PET, as well as no ionizing radiation dose to patients. Whole-body DWI is also promising for treatment response assessment in bone metastases, a critical area where CT and bone scan are inadequate (8–11).

Despite its advantages, DWI suffers from technical limitations that limit its clinical adoption. One limitation is distortion induced by static magnetic field (B0) inhomogeneity. This distortion is inevitably present in echo-planar imaging techniques used to collect DWI (12). These distortion artifacts can cause substantial warping of images and, thus, affect image guidance for radiation therapy, surgery, and targeted biopsy, which all rely on accurate spatial localization of bone metastases. Treatment response assessment also depends on accurate measurement of bone lesions (8, 11). Several techniques have been developed to measure and correct for these artifacts (13–15), but none has yet been widely adopted for routine clinical use.

For DWI of prostate and breast tissue, distortion correction using the reverse polarity gradient (RPG) technique (14) has been shown to improve anatomic localization (16, 17). However, the impact of these distortions has not yet been explored in the context of bone metastases or whole-body DWI acquisitions.

In this study, we investigate whether B0 inhomogeneities lead to DWI distortions that affect localization of bone metastases in whole-body magnetic resonance imaging (WB-MRI) data. We aimed to use RPG to measure the distortion in the diffusion signal of bone metastases, as well as the distortion in the diffusion signal of various skeletal landmarks. We also sought to determine whether correcting for these distortions with RPG would improve anatomic correlation of DWI with T2-weighted images.

Methods

Study Population

Patients with suspected or known metastatic prostate cancer were enrolled on a prospective observational non-contrast whole-body MRI trial at the University of California San Diego (IRB #151686) from August 2017 to March 2020. All study participants provided informed consent. In this study, we analyzed the subset of trial participants who had evidence of bone metastases on DWI.

Image Acquisition and Processing

Whole-body MRI was acquired on a 3.0 T MRI system (Discovery MR750, GE Healthcare, Waukesha, WI, USA) with a multi-parametric MRI protocol that included T2-weighted (TE/TR: 113/1350 ms, acquisition matrix: 384×224, resampled matrix: 512×512, FOV: 400 x 400 mm, slices: 46, slice thickness: 6 mm) and DWI (TE/TR: 75/4750 ms, acquisition matrix: 80×80, resampled matrix: 128×128, FOV: 400 x 400 mm, slices: 46, slice thickness: 6 mm). The DWI protocol included diffusion weightings (b-values) of 0, 500, 1000, and 2000 s/mm^2, with 1, 6, 6, and 12 diffusion directions, respectively. Each subject underwent this protocol at 5 different stations to produce a whole-body image. Stations 1, 2, 3, 4, and 5 included, respectively, the head, neck and thorax, abdomen, pelvis, and upper legs. This protocol did not use respiratory gating.

In order to estimate the distortion due to B0 inhomogeneity using RPG, b=0 s/mm^2 images were acquired in both the forward and reverse phase encoded direction. The collection of the additional b=0 s/ mm^2 image added 30 to 40 seconds to the protocol at each imaging station. The RPG algorithm has been described previously in detail (14). Briefly, the forward and reverse

images are smoothed and registered with one another. This registration is used to calculate an initial estimate of the distortion. This procedure is then repeated several times, and, in each iteration, the smoothing is performed with a thinner kernel and the distortion estimate is refined. The result of this procedure is a 3D distortion map where each value in the volume represents the number of voxels it was displaced in the phase encoding direction due to B0 inhomogeneity. This distortion map can be applied to the raw diffusion images for distortion correction (DisCo). B0-related distortion is independent of diffusion weighting, so this map can be used to correct the entire diffusion dataset to produce post-DisCo images.

Lesions identified as bone metastases were annotated manually on the diffusion images in MIM (MIM Software Inc, Cleveland, OH, USA) by a radiation oncologist (C.H.F.). Standard-of-care clinical imaging was also used to inform DWI lesion delineation, where applicable. These annotations were then reviewed and confirmed by a fellowship-trained body radiologist (M.E.H.). Only Stations 2, 3, and 4, were used in our analyses, as very few bone metastases were found in Stations 1 and 5. We refer to Stations 2, 3, and 4 as the Thorax, Abdomen, and Pelvis Station in the rest of this report.

Statistical Analysis

Estimating Distortion of Bone Metastases

For each lesion, we identified the horizontal slice in which the lesion was largest and selected it for analysis. Within that horizontal slice, a rectangular bounding box was drawn around each lesion, with the boundaries drawn 10 voxels from the lateral edge (in diffusion MRI space) of the lesion (for example, see Figure 1). The bounding box was then overlaid onto the distortion map. To quantify the extent to which distortion occurred within the lesion and in the

immediate surrounding area, the RMS within the box was calculated using the following formula, as described previously (16):

$$RMS_{distortion} = 2 \times \sqrt{\mu_{distortion}^2 + \sigma_{distortion}^2}$$

where $\mu_{distortion}$ and $\sigma_{distortion}$ represent the mean and standard deviation of the distortion values of the voxels within the bounding box. We further generated 1000 bootstrap samples to obtain a 95% confidence interval for the mean RMS. We report the mean RMS observed, as well as the 95% confidence intervals.

Assessing Similarity between Diffusion and Structural Images

The above analysis uses DisCo to estimate the displacement of lesions in uncorrected images. Next, we conducted a mutual information analysis to assess the degree to which DisCo produces diffusion images more faithfully reflect underlying anatomy of the T2-weighted images. The T2 image for each subject was resampled to match the resolution of the DWI images. For each lesion, we computed the normalized mutual information (MI) between the pre-DisCo b=0 image and T2 image, and the normalized MI between the post-DisCo b=0 image and T2 image. MI values were calculated for the entire horizontal slice (17). We compared pre-DisCo and post-DisCo MI values with a Wilcoxon signed-rank test, with each lesion representing an observation. This Wilcoxon signed-rank analysis was then repeated for only the subset of lesions within each imaging station. P-values less than 0.05 were considered significant.

Estimating Distortion of Skeletal Landmarks

To characterize distortions across the skeleton, beyond the specific set of bone metastases in our dataset, we annotated several landmarks that sampled various parts of the skeleton on the structural T2-weighted MRIs. These landmarks included: most anterior point of the femoral head and the most posterior point of three different vertebrae (T3, T12, and S1) at a level midway between the superior and inferior edges of the vertebral body. Then, a bounding box was drawn around each landmark with boundaries 4 voxels away in the left, right, anterior, and posterior direction, and 2 voxels away in the superior and inferior direction. To estimate the distortion at and near the landmark, the RMS within the box was calculated using the above formula. We selected 10 random subjects for this complete manual landmark annotation. Again, mean and bootstrap-derived confidence intervals are reported. Visual inspection of the distortion maps from our sample suggest that distortions are generally symmetric, so, left and right values for the femoral head are displayed and were analyzed together.

Calculating Error Reduction After DisCo

Lastly, we aimed to complement the above mutual information analysis with a more interpretable measure of the extent to which DisCo improved the similarity between diffusion and structural images. For each patient, we annotated landmarks separately on their pre-DisCo b=0, post-DisCo b=0, and T2 images. We again included the anterior point of the femoral head as a landmark. For this anterior point of femoral head landmark, we calculated the distance between the pre-DisCo b=0 point annotation and the T2 point annotation as a measure of error. We then calculated the distance between the post-DisCo b=0 point annotation and the T2 point annotation in order to calculate the change in error after DisCo. We report the mean changes in error after distortion correction, as well as bootstrap-derived confidence intervals. For the

vertebrae, rather than selecting individual vertebrae, we traced the entire posterior edge of the vertebral column in the mid-sagittal plane in each imaging station (for example, see Figure 4) and calculated changes in error at each horizontal slice (the 3 superior- and 3- inferior most horizontal slices were ignored since the FOV begins to taper off at these edges of the volume). In these analyses, a negative error change denotes an error reduction and, thus, better agreement between b=0 and T2 images. To summarize our findings from these analyses we plotted the distributions of vertebral error reductions (Figure 5). Further, for each imaging station, we aggregated all of the vertebral error change values across all participants and report the mean with bootstrap-derived confidence intervals. This analysis was performed in the same subset of 10 participants used for the anatomic landmark RMS analysis.

Results

Our study included 18 participants with bone metastases on DWI over 19 scans (1 had longitudinal data and thus, 2 scans). Across the entire sample, 77 individual lesions were defined and included for analysis. In the Thorax Station, lesions were primarily found in ribs, clavicles, scapulae, and vertebrae. Abdomen Station lesions were primarily in the vertebrae, and Pelvis Station lesions were found in pelvic bones and femurs.

Estimating Distortion of Bone Metastases

The maximum RMS was 17.1 mm and was observed in a clavicular lesion in the Thorax Station. In the Abdomen and Pelvis Station, the maximum RMS values were 14.6 mm and 10.9 mm, respectively. Across all lesions, the average RMS was 5.6 mm (95% CI: 4.8-6.5). When grouped by station, the mean RMS for Thorax, Abdomen, and Pelvis Stations were 8.1 mm (95% CI: 6.3-9.8), 6.1 mm (95% CI: 4.3-8.3), and 3.7 mm (95% CI: 3.0-4.6), respectively. Examples of vertebral and femoral lesions are displayed in Figure 2. The distributions of RMS values are illustrated in Figure 3.

Assessing Similarity between Diffusion and Structural Images

In the MI analysis, applying DisCo led to consistently increased MI between the DWI b=0 s/mm^2 and T2 image. When comparing the pre-DisCo MI values to the post-DisCo MI values with Wilcoxon signed-rank tests, we found that the post-DisCo MI values were significantly higher ($p<10^{-13}$). The change in MI values after applying DisCo are displayed in Figure 3. This association was also consistent for each imaging stations (Thorax Station: $p<10^{-4}$, Abdomen Station: $p=0.002$, Pelvis Station: $p<10^{-6}$).

Estimating Distortion of Skeletal Landmarks

Across all landmarks in the RMS skeletal landmark analysis, we observed an average estimated distortion of 6.3 mm. The landmark at T3 had the highest average distortion at 19.3 mm (95% CI: 14.7-23.5). The T12 and S1 landmarks had an average distortion of 4.3 mm (95% CI: 2.8-5.6) and 3.4 mm (95% CI: 1.5-5.7), respectively. Lastly, the average estimated distortion of the femoral head landmark was 2.6 mm (95% CI: 2.1-3.0). The RMS values for these skeletal landmarks are displayed in Figure 5a.

Calculating Error Reduction After DisCo

Application of RPG led to reductions in error between landmarks defined on both DWI b=0 s/mm^2 and T2 images. For the anterior femur landmark, the mean [95% CI] error between the pre-DisCo b=0 s/mm^2 and T2 annotations was 3.7 mm [2.5, 4.8]. The mean [95% CI] error between post-DisCo b=0 s/mm^2 and T2 annotations was 2.5 mm [1.8, 3.1]. Thus, application of DisCo led to a mean change in error of [95% CI] of -1.2 mm [-2.1,-0.4].

For the vertebral landmarks, the distributions of error changes for each participant are plotted in Figure 5b. The mean error [95% CI] prior to application of DisCo for the thoracic, abdominal, and pelvic vertebrae, respectively, were 7.2 mm [6.6, 7.8], 3.5 mm [3.3, 3.8], and 3.2 mm [2.7, 3.7]. After the application of of DisCo, the errors for these vertebrae were 3.4 mm [3.1, 3.6], 2.6 mm [2.3, 2.8], and 2.6 mm [2.1, 3.2]. The mean change in error [95% CI] for the thoracic, abdominal, and pelvic vertebrae were -3.8 mm [-4.3,-3.3], -1.0 mm [-1.2,-0.7], and -0.6 mm [-1.0,-0.17], respectively. The largest observed error reductions for thoracic, abdominal, and pelvic vertebrae, respectively, were -18.0, -18.0, and -5.5 mm (Figure 5).

Discussion

We measured displacement of bone metastases on uncorrected DWI of up to 17 mm, with mean displacement of 5.6 mm (95% CI: 4.8-6.5 mm). Estimated distortion from B0 inhomogeneity was greatest in the Thorax Station and smallest in the Pelvis Station. Correction of this distortion improved anatomic accuracy of DWI and improved correlation with anatomy on T2-weighted images. This distortion may be meaningful in some clinical applications, including image-guided bone biopsy and precision radiotherapy. As DWI is often superior for delineation of cancer (18), corrected DWI might facilitate diagnostic and therapeutic procedures that require high precision. Similarly, DWI has promise as a longitudinal biomarker of treatment response (19), another clinical application where anatomic accuracy may prove important.

Prior studies have demonstrated that B0 inhomogeneities affect organ or lesion localization in the prostate and breast (16, 17, 20). The extent of B0 inhomogeneities and their consequent artifacts depend, in part, on the anatomic environment of a lesion (e.g. how close the lesion is to an air-tissue interface). Our findings here suggest that, like prostate and breast, bone is also susceptible to meaningful distortion. As illustrated in Figure 3, bone metastases underwent displacement of up to 17, 14, and 10 mm in the Thorax, Abdomen, and Pelvis Station, respectively. This amounts to several voxels of displacement within the image and could potentially lead to missing a target on guided biopsy or stereotactic radiation therapy—or, if the distortion is grossly apparent, it could lead to exclusion of DWI from direct use in planning for these procedures, thus excluding one of the most sensitive imaging modalities for bone metastases (9, 21, 22). The elevated RMS values in the Thorax Station, relative to the other imaging stations, may be due to a number of factors. As previously noted, proximity to air-tissue interfaces can exacerbate distortion. The Thorax Station is where imaging of rib, clavicle, and

shoulder bones takes place. Since these bones are all close to air-tissue interfaces, there are several places within the FOV of the Thorax Station where bone metastases are prone to heavy distortion. However, the ribs, clavicles, and sternum are also subject to respiratory motion, and we are not able to separate these effects in this study. Future studies might benefit from controlling for respiratory motion, such as abdominal compression, active breathing control, or respiratory gating (23). Nevertheless, we found that the vertebrae of the Thorax Station, which are less affected by respiratory motion, still exhibited elevated RMS suggesting that not all of the distortion observed in the Thorax Station in our study can be explained by respiratory motion.

In addition to biopsy or radiation planning, another potential application of DWI is in assessing response to therapy (19). In a 2014 study, investigators found that changes in overall tumor volume as measured by whole-body DWI correlated with treatment response in breast and prostate cancer patients with bone metastases (8). As demonstrated in Figure 1C, voxels undergo varying levels of displacement along the phase-encoding gradient. Fluctuating amounts of distortion within and around a lesion can lead to contraction, expansion, or other geometric distortion of the lesion. The metastasis in the left femoral head that we show in Figure 2E-H underwent B0 inhomogeneity induced contraction, as can be appreciated with the dark strip of voxels at the anterior edge of the lesion in Figure 2G. The right clavicular lesion in Figure 1 also clearly underwent geometric distortion. Artificial geometric distortions like these may lead to misinterpretations in patients' responses to therapy, such as mistaking contraction or expansion due to B0 inhomogeneity for tumor shrinkage or growth.

There are several tools available to correct for these artifacts and reduce the likelihood of missing a target or misinterpreting treatment response (13–15). In the RPG method used here, a correction that can be applied to the diffusion dataset is simultaneously generated while

calculating the voxel-wise displacements; this method was chosen for its efficiency, as little scan time (30-40 seconds per station) was required. A salient question, however, is whether this correction actually produces images that more accurately reflect anatomy. The consistent increases in MI between DWI b=0 and T2 images after DisCo is in line with prior work that performed MI-based analyses in other organs (17, 20). We further showed that applying RPG can lead to reduction in error between anatomic landmarks annotated on diffusion and structural images (Figure 5). We did observe some instances of small increases in measured error after the application of RPG, which may be due to actual movement of the patient or internal organs (e.g., via breathing or peristalsis) between DWI and T2 acquisitions. Nevertheless, the net effect of RPG was to consistently reduce measured errors. Taken together, our findings suggest that the RPG method is capable of generating diffusion images that more closely represent the true anatomy.

Limitations

One limitation of our study is that it only included prostate cancer patients. Bone is also a common site of metastases in other cancers, particularly lung and breast cancer. DWI has been successfully used to visualize bone metastases in other cancers (for breast see (8); for melanoma, see (24)). Lesion appearance may vary on DWI by cancer type, but there is no *a priori* reason to suspect that distortion effects would be substantially affected by cancer histology. The effect of respiration on our distortion estimates is a noteworthy technical limitation. In addition to respiratory motion, which we have discussed above, slight differences in respiratory volume can also lead to artifacts. Thus, even if image acquisition were gated with the respiratory cycle, it is likely that some residual distortion would remain. Our group is actively working on imaging

protocols and processing methods to address this residual distortion that is relevant not only to imaging of bones near the lungs, but also to imaging of other organs near the lungs, such as the liver and pancreas. Finally, we note that our whole-body imaging protocol does not capture the bones of the distal extremities; metastases distal to the elbow and knee, however, are relatively uncommon.

Conclusions

In summary, we found that B0 inhomogeneity results in distortion of whole-body diffusion images that leads to artifactual displacement of bone and bone metastases. These distortions may be severe enough to interfere with accurate biopsy or stereotactic treatment. Moreover, these distortions could complicate interpretation of tumor shrinkage or growth. The RPG technique used here is efficient (only 30-40 seconds additional scan time per station) and reduced distortion artifacts in whole-body DWI.

References

1. Mundy GR: Metastasis to bone: causes, consequences and therapeutic opportunities. *Nat Rev Cancer* 2002; 2:584–593.

2. Schulman KL, Kohles J: Economic burden of metastatic bone disease in the U.S. *Cancer* 2007; 109:2334–2342.

3. Coleman RE: Clinical features of metastatic bone disease and risk of skeletal morbidity. *Clin Cancer Res Off J Am Assoc Cancer Res* 2006; 12(20 Pt 2):6243s–6249s.

4. Qu X, Huang X, Yan W, Wu L, Dai K: A meta-analysis of ^{18}FDG-PET-CT, ^{18}FDG-PET, MRI and bone scintigraphy for diagnosis of bone metastases in patients with lung cancer. *Eur J Radiol* 2012; 81:1007–1015.

5. Yang H-L, Liu T, Wang X-M, Xu Y, Deng S-M: Diagnosis of bone metastases: a meta-analysis comparing ^{18}FDG PET, CT, MRI and bone scintigraphy. *Eur Radiol* 2011; 21:2604–2617.

6. Eiber M, Holzapfel K, Ganter C, et al.: Whole-body MRI including diffusion-weighted imaging (DWI) for patients with recurring prostate cancer: Technical feasibility and assessment of lesion conspicuity in DWI. *J Magn Reson Imaging* 2011; 33:1160–1170.

7. Jambor I, Kuisma A, Ramadan S, et al.: Prospective evaluation of planar bone scintigraphy, SPECT, SPECT/CT, ^{18} F-NaF PET/CT and whole body 1.5T MRI, including DWI, for the detection of bone metastases in high risk breast and prostate cancer patients: SKELETA clinical trial. *Acta Oncol* 2016; 55:59–67.

8. Blackledge MD, Collins DJ, Tunariu N, et al.: Assessment of Treatment Response by Total Tumor Volume and Global Apparent Diffusion Coefficient Using Diffusion-Weighted MRI in Patients with Metastatic Bone Disease: A Feasibility Study. *PLoS ONE* 2014; 9:e91779.

9. Lecouvet FE, Talbot JN, Messiou C, Bourguet P, Liu Y, de Souza NM: Monitoring the response of bone metastases to treatment with Magnetic Resonance Imaging and nuclear medicine techniques: A review and position statement by the European Organisation for Research and Treatment of Cancer imaging group. *Eur J Cancer* 2014; 50:2519–2531.

10. Perez-Lopez R, Lorente D, Blackledge MD, et al.: Volume of Bone Metastasis Assessed with Whole-Body Diffusion-weighted Imaging Is Associated with Overall Survival in Metastatic Castration-resistant Prostate Cancer. *Radiology* 2016; 280:151–160.

11. Perez-Lopez R, Mateo J, Mossop H, et al.: Diffusion-weighted imaging as a treatment response biomarker evaluating bone metastases in prostate cancer: a pilot study. *Radiology* 2017; 283:168–177.

12. Bihan DL, Poupon C, Amadon A, Lethimonnier F: Artifacts and pitfalls in diffusion MRI. *J Magn Reson Imaging* 2006; 24:478–488.

13. Andersson JLR, Skare S, Ashburner J: How to correct susceptibility distortions in spin-echo echo-planar images: application to diffusion tensor imaging. *NeuroImage* 2003; 20:870–888.

14. Holland D, Kuperman JM, Dale AM: Efficient correction of inhomogeneous static magnetic field-induced distortion in Echo Planar Imaging. *NeuroImage* 2010; 50:175–183.

15. Jezzard P, Balaban RS: Correction for geometric distortion in echo planar images from B0 field variations. *Magn Reson Med* 1995; 34:65–73.

16. Rakow-Penner RA, White NS, Margolis DJA, et al.: Prostate diffusion imaging with distortion correction. *Magn Reson Imaging* 2015; 33:1178–1181.

17. Teruel JR, Fjøsne HE, Østlie A, et al.: Inhomogeneous static magnetic field-induced distortion correction applied to diffusion weighted MRI of the breast at 3T. *Magn Reson Med* 2015; 74:1138–1144.

18. Hou D-L, Shi G-F, Gao X-S, et al.: Improved longitudinal length accuracy of gross tumor volume delineation with diffusion weighted magnetic resonance imaging for esophageal squamous cell carcinoma. *Radiat Oncol* 2013; 8:169.

19. Padhani AR, Gogbashian A: Bony metastases: assessing response to therapy with whole-body diffusion MRI. *Cancer Imaging* 2011; 11:S129–S145.

20. Rodríguez-Soto AE, Park H, Holland D, et al.: Correction of Artifacts Induced by B0 Inhomogeneities in Breast MRI using Reduced Field-of-View Echo-Planar Imaging and Enhanced Reverse Polarity Gradient Method. :17.

21. Lecouvet FE, El Mouedden J, Collette L, et al.: Can Whole-body Magnetic Resonance Imaging with Diffusion-weighted Imaging Replace Tc 99m Bone Scanning and Computed Tomography for Single-step Detection of Metastases in Patients with High-risk Prostate Cancer? *Eur Urol* 2012; 62:68–75.

22. Luboldt W, Küfer R, Blumstein N, et al.: Prostate Carcinoma: Diffusion-weighted Imaging as Potential Alternative to Conventional MR and C-Choline PET/CT for Detection of Bone Metastases. *Radiology* 2008; 249:1017–1025.

23. Brandner ED, Chetty IJ, Giaddui TG, Xiao Y, Huq MS: Motion Management Strategies and Technical Issues Associated with Stereotactic Body Radiotherapy of Thoracic and Upper Abdominal Tumors: A Review from NRG Oncology. *Med Phys* 2017; 44:2595–2612.

24. Larbi A, Omoumi P, Pasoglou V, et al.: Whole-body MRI to assess bone involvement in prostate cancer and multiple myeloma: comparison of the diagnostic accuracies of the T1, short tau inversion recovery (STIR), and high b-values diffusion-weighted imaging (DWI) sequences. *Eur Radiol* 2019; 29:4503–4513.

Figures

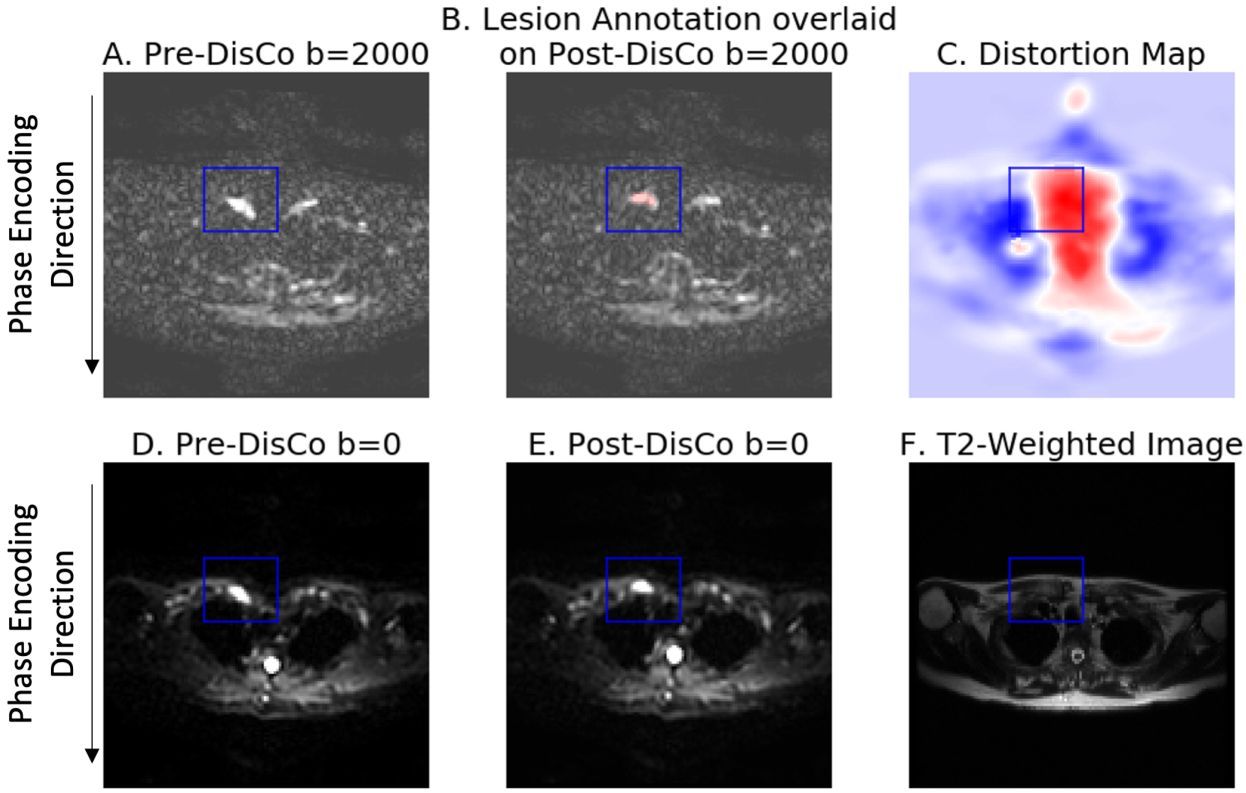

Figure 1. Example bone metastasis illustrating effect of B0 inhomogeneity induced distortion on DWI. In each subfigure, the slice corresponds to the horizontal slice at which the lesion is the largest (see Methods). The blue bounding box was drawn 10 voxels from the lateral edge of the lesion (in DWI space) in each of the 4 directions, then overlaid on the other images. A. Average b=2000 s/mm^2 image prior to DisCo. B. Lesion annotation (pink) overlaid onto b=2000 s/mm^2 image after DisCo. C. Estimation of the distortion within the slice. Voxel values represent the extent of displacement undergone by each voxel. Red and blue values denote displacement in the posterior and anterior direction, respectively. D. Average b=0 s/mm^2 image prior to DisCo. E. Average b=0 s/mm^2 image after DisCo. F. T2-weighted image at the same slice. Abbreviations: DisCo=distortion correction.

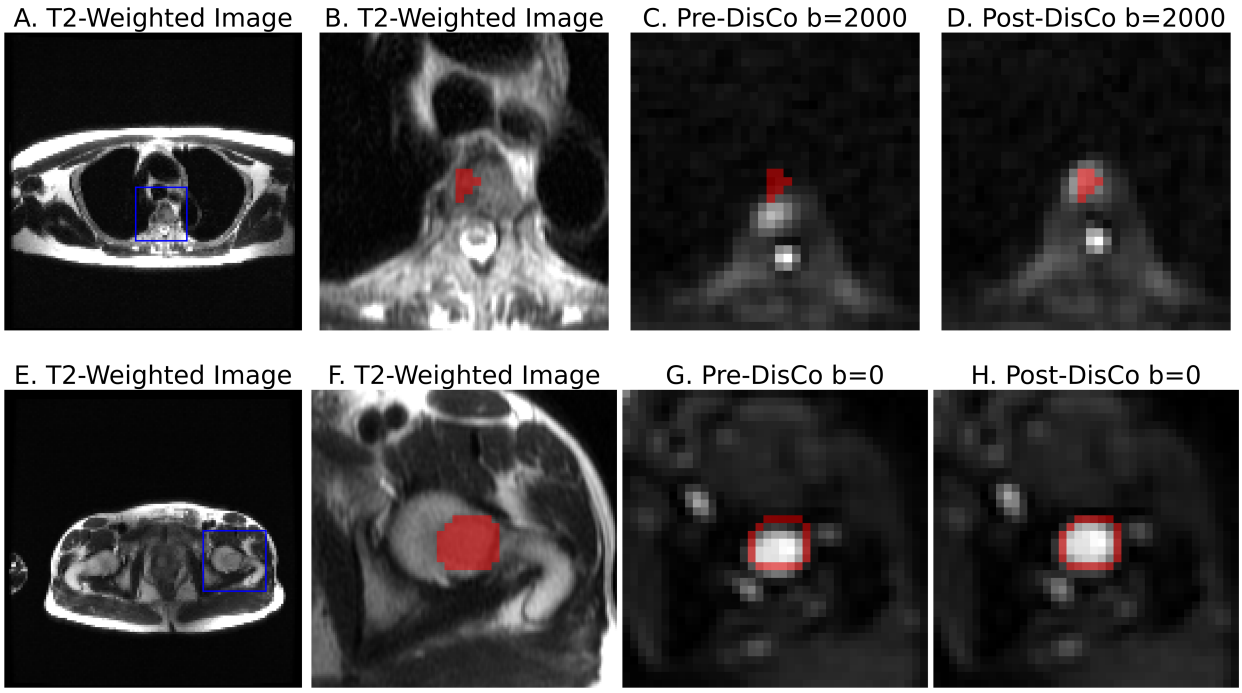

Figure 2. Examples of bone metastases as seen on b=0 s/mm^2 DWI pre-and post-DisCo. The top row (A-D) shows a vertebral lesion in the Thorax Station. The bottom row (E-H) shows a lesion within the left femoral head in the Pelvis Station. **(**A,E) T2-weighted images at the corresponding level with blue bounding box drawn around lesion. (B, F) T2-weighted images zoomed in to visualize lesion and surrounding area. (C, G) Zoomed in DWI b=2000 s/mm^2 and b=0 s/mm^2 images before DisCo, respectively. (D, H) Zoomed in DWI b=0 s/mm^2 images after DisCo. Outlines of the lesion annotations are overlaid in red. In both examples, the lesions were translated anteriorly following DisCo. Without DisCo, lesion localization may have erred posteriorly. Abbreviations: DisCo=distortion correction.

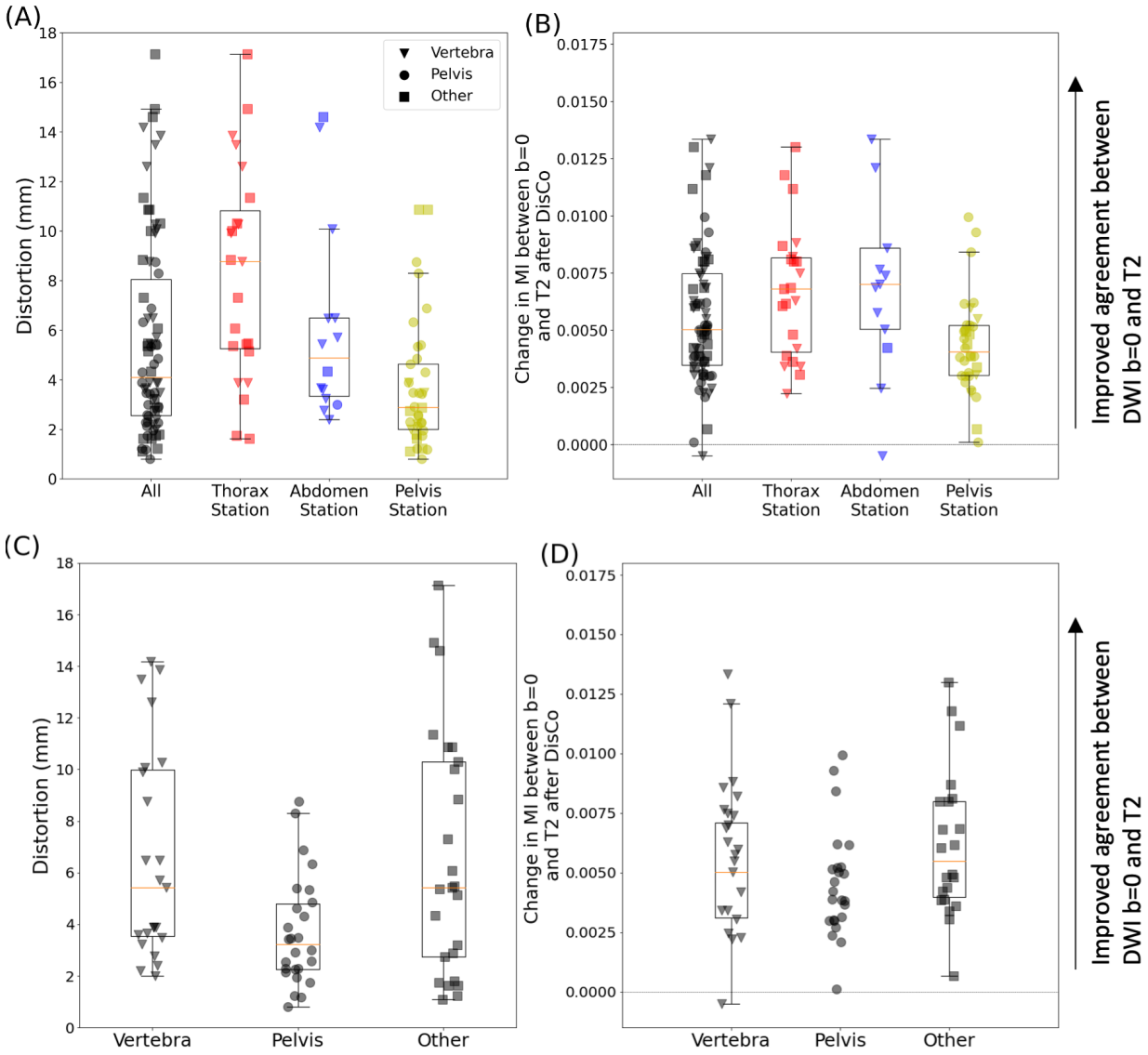

Figure 3. Distribution of RMS of distortion and MI between b=0 s/mm^2 and T2-weighted images. (A) Distortion for lesions across all stations (black) as well as the distribution within specific imaging Stations (red, blue, and yellow). Distortion was estimated by calculating the RMS of the values in the distortion map that correspond to the lesion annotation and immediately surrounding areas (see Methods). (B) Change in MI values between the DWI b=0 s/mm^2 and T2-weighted images after DisCo. A value larger than 0 indicates improved agreement between DWI b=0 and T2-weighted images. Again, we plot the distribution for all lesions as well as the breakdown for different Stations. (C) Distortion for lesions broken down by anatomic group. (D) Change in MI values between the DWI b=0 s/mm^2 and T2-weighted images after DisCo broken down by anatomic group. DisCo led to consistent increases in similarity between DWI b=0 s/mm^2 and T2-weighted images. Abbreviations: RMS=root mean square, MI=mutual information.

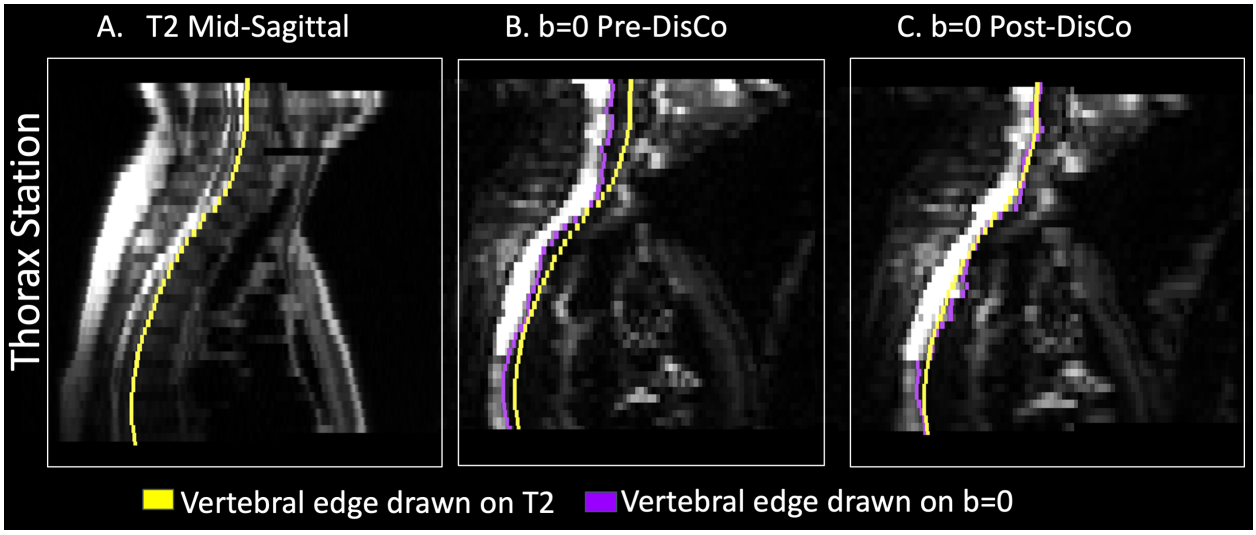

Figure 4. Example of tracing of posterior border of vertebrae for error change analysis. (A) Mid-sagittal slice of T2-weighted MRI from the Thorax Station for a single subject. The yellow represents the annotation of the posterior edge of the vertebral column on the T2. (B) Mid-sagittal slice of the DWI b=0 s/mm^2 prior to DisCo. The purple in this panel represents the annotation of the posterior edge of the vertebral column on the pre-DisCo DWI b=0 s/mm^2 (C) Mid-sagittal slice of DWI b=0 s/mm^2 after DisCo. The purple in this panel represents the annotation of the posterior edge of the vertebral column on the post-DisCo DWI b=0 s/mm^2. The average distance between the yellow and purple tracings (i.e., the error) decreases after application of DisCo. Abbreviations: DisCo=distortion correction.

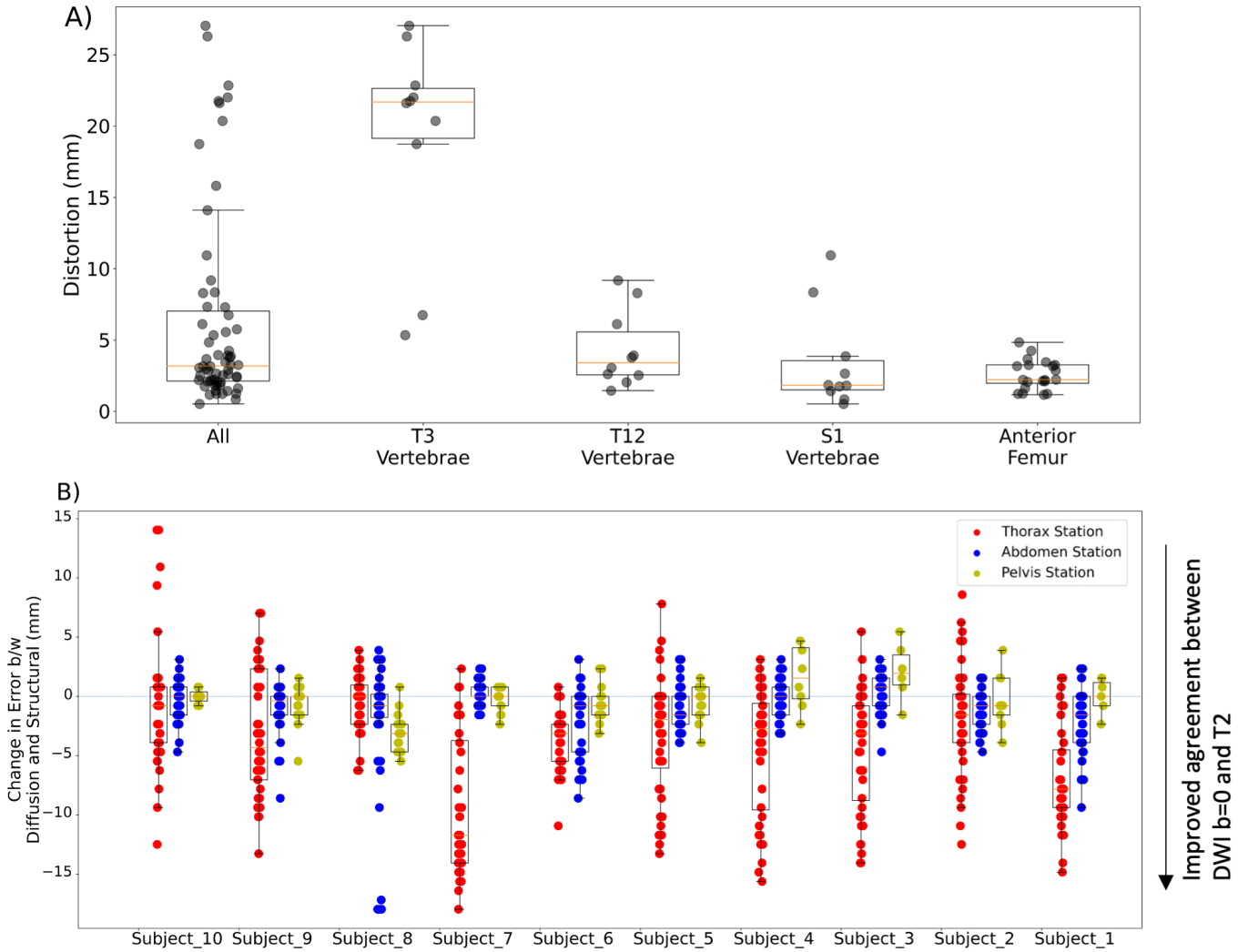

Figure 5. Results from anatomic landmark analysis. (A) Distortion of various anatomic landmarks. Distortion was estimated by calculating the RMS of the values in the distortion map that correspond to the lesion annotation and immediately surrounding areas. For the vertebrae, the landmark was the most posterior point of the vertebral body in the mid-sagittal plane at a level half-way between the superior and inferior edges of the vertebral body. For the femur, the landmark was the most anterior point. (B) Distribution of changes in error between the DWI b=0 s/mm^2 annotation and the T2 annotation of the vertebral posterior vertebral borders. For each subject, 40 points are plotted for the Thorax and Abdomen Stations, corresponding to 40 horizontal slices within that Station. The Pelvis Station has fewer points because the vertebral column does not span the entire imaging station. Application of RPG DisCo led to error reductions, particularly in the vertebrae of the Thorax Station. Abbreviations: RMS=root mean square.